



Sodium channel kinetic changes that produce Brugada syndrome or progressive cardiac conduction system disease

Zhu-Shan Zhang, Joseph Tranquillo, Valentina Neplioueva, Nenad Bursac and Augustus O. Grant

Am J Physiol Heart Circ Physiol 292:399-407, 2007. First published Jul 28, 2006;
doi:10.1152/ajpheart.01025.2005

You might find this additional information useful...

Supplemental material for this article can be found at:

<http://ajpheart.physiology.org/cgi/content/full/01025.2005/DC1>

This article cites 21 articles, 12 of which you can access free at:

<http://ajpheart.physiology.org/cgi/content/full/292/1/H399#BIBL>

Updated information and services including high-resolution figures, can be found at:

<http://ajpheart.physiology.org/cgi/content/full/292/1/H399>

Additional material and information about *AJP - Heart and Circulatory Physiology* can be found at:

<http://www.the-aps.org/publications/ajpheart>

This information is current as of January 26, 2007 .

AJP - Heart and Circulatory Physiology publishes original investigations on the physiology of the heart, blood vessels, and lymphatics, including experimental and theoretical studies of cardiovascular function at all levels of organization ranging from the intact animal to the cellular, subcellular, and molecular levels. It is published 12 times a year (monthly) by the American Physiological Society, 9650 Rockville Pike, Bethesda MD 20814-3991. Copyright © 2005 by the American Physiological Society. ISSN: 0363-6135, ESN: 1522-1539. Visit our website at <http://www.the-aps.org/>.



Sodium channel kinetic changes that produce Brugada syndrome or progressive cardiac conduction system disease

Zhu-Shan Zhang,¹ Joseph Tranquillo,³ Valentina Neplioueva,¹ Nenad Bursac,² and Augustus O. Grant¹

Departments of ¹Medicine and ²Biomedical Engineering, Duke University, Durham, North Carolina; and

³Department of Biomedical and Electrical Engineering, Bucknell University, Lewisburg, Pennsylvania

Submitted 27 September 2005; accepted in final form 23 June 2006

Zhang, Zhu-Shan, Joseph Tranquillo, Valentina Neplioueva, Nenad Bursac, and Augustus O. Grant. Sodium channel kinetic changes that produce Brugada syndrome or progressive cardiac conduction system disease. *Am J Physiol Heart Circ Physiol* 292: H399–H407, 2007. First published July 28, 2006; doi:10.1152/ajpheart.01025.2005.—Some mutations of the sodium channel gene $Na_{v1.5}$ are multifunctional, causing combinations of LQTS, Brugada syndrome and progressive cardiac conduction system disease (PCCD). The combination of Brugada syndrome and PCCD is uncommon, although they both result from a reduction in the sodium current. We hypothesize that slow conduction is sufficient to cause S-T segment elevation and undertook a combined experimental and theoretical study to determine whether conduction slowing alone can produce the Brugada phenotype. Deletion of lysine 1479 in one of two positively charged clusters in the III/IV inter-domain linker causes both syndromes. We have examined the functional effects of this mutation using heterologous expression of the wild-type and mutant sodium channel in HEK-293-EBNA cells. We show that $\Delta K1479$ shifts the potential of half-activation, $V_{1/2m}$, to more positive potentials ($V_{1/2m} = -36.8 \pm 0.8$ and -24.5 ± 1.3 mV for the wild-type and $\Delta K1479$ mutant respectively, $n = 11, 10$). The depolarizing shift increases the extent of depolarization required for activation. The potential of half-inactivation, $V_{1/2h}$, is also shifted to more positive potentials ($V_{1/2h} = -85 \pm 1.1$ and -79.4 ± 1.2 mV for wild-type and $\Delta K1479$ mutant respectively), increasing the fraction of channels available for activation. These shifts are quantitatively the same as a mutation that produces PCCD only, G514C. We incorporated experimentally derived parameters into a model of the cardiac action potential and its propagation in a one dimensional cable (simulating endo-, mid-myocardial and epicardial regions). The simulations show that action potential and ECG changes consistent with Brugada syndrome may result from conduction slowing alone; marked repolarization heterogeneity is not required. The findings also suggest how Brugada syndrome and PCCD which both result from loss of sodium channel function are sometimes present alone and at other times in combination.

sodium channel; Brugada syndrome; conduction system disease

PROGRESSIVE CARDIAC CONDUCTION SYSTEM DISEASE (PCCD) and a subset of Brugada syndrome are allelic disorders. They may result from mutations in the α -subunit of the cardiac sodium channel gene, $Na_{v1.5}$. The fundamental defect that may produce both syndromes falls into the following two categories 1) synthesis of a nonfunctional protein or failure of membrane insertion of the synthesized protein or 2) changes in channel kinetics that reduce the inward sodium current during *phases 0* and *1* of the action potential (3, 21, 27). In a subset of patients with Brugada syndrome, reduction of the sodium current during late *phase 0* and early *phase 1* shifts the action potential current-voltage trajectory in the outward direction. This exaggerates the normal epicardial to endocardial repolarization

gradient that is most prominent at the base of the right ventricle. The exaggerated gradient yields the S-T segment elevation in the right precordial leads and produces *phase 2* reentry (10). The subset of patients with Brugada syndrome on the basis of sodium channel mutations also shows evidence of conduction impairment, including prolongation of the PQ and HV intervals (24). PCCD arises when channel availability is reduced at the normal resting potential or when maximal channel activation requires increased depolarization. The conduction disturbance is observed as right bundle branch block, left bundle branch block or complete heart block, or as block at the level of the sinoatrial or atrioventricular nodes (21).

Schulze-Bahr et al. (22) recently described a kindred in which both Brugada syndrome and PCCD resulted from the deletion of a single lysine residue, K1479, in the III-IV interdomain linker. We considered an analysis of the kinetic effects of this mutation potentially informative for two reasons. K1479 is one of 12 positively charged residues in the III-IV interdomain linker. This 53-residue segment is the most highly conserved region of sodium channels. The linker has a density of charged residues similar to that of the S_4 segment, a region that functions as the voltage sensor during channel activation. NMR and molecular dynamics studies suggest that the charged residues are concentrated in two α -helical clusters in a hairpin motif (20, 23); K1479 is located in the first of these clusters. K1500 is located in the second (downstream) cluster. The deletion of K1500 resulted in long QT syndrome (LQTS), Brugada syndrome, and PCCD (9). Initial structure-function studies suggested that the III/IV linker functions as the fast inactivation gate. We and others (9) have shown that the charged residues in the second cluster of the linker may play a role in the coupling of activation and inactivation. The role of the residues in the first cluster that includes K1479 has not been examined.

When expressed in human embryonic kidney cells, the K1479 deletion sodium channel mutant yielded robust currents with altered kinetics. Depolarizing voltage shifts were observed for both the conductance and inactivation-voltage relationships. For the sodium channel mutant that causes PCCD on the basis of a change in kinetics, Tan et al. (25) observed a depolarizing shift in both the conductance- and inactivation-voltage relationships. They suggested that the opposing effects of those shifts on sodium current amplitude were the reasons that Brugada syndrome was not observed in their kindred. We performed simulations to determine the interplay between the positive shift in the conduction-voltage (G - V) relationships (tending to reduce sodium current) and the positive shift in the

Address for reprint requests and other correspondence: A. O. Grant, Duke Univ. Medical Center, Box 3504, Durham, NC 27710 (e-mail: grant007@mc.duke.edu).

The costs of publication of this article were defrayed in part by the payment of page charges. The article must therefore be hereby marked "advertisement" in accordance with 18 U.S.C. Section 1734 solely to indicate this fact.

inactivation-voltage relationships (enhancing the fraction of available sodium channels at the normal resting potential) in the production of conduction slowing and action potential changes consistent with Brugada syndrome.

METHODS

Preparation of cell lines expressing the WT and mutant sodium channels. The human cardiac sodium channel gene *hH1* was cloned into the mammalian expression plasmid pcDNA3.1-Hygro⁺ (Invitrogen). The K1479 deletion (Δ K1479) in the III-IV interdomain linker of the α -subunit of the sodium channel was performed using recombinant PCR (12). Fidelity of the mutation was documented by direct sequencing. Human embryonic kidney cells (293-EBNA) were transfected with the plasmids pcDNA3.1/hH1 and pcDNA3.1/hH1 Δ K1479 using lipofectamine. Stable cell lines were established in HEK-293-EBNA cells using hygromycin as the dominant selective marker. The wild type (WT) and Δ K1479 mutant α -subunits expressed current of several nanoamperes in the HEK-293-EBNA cells.

Experimental setup. Whole cell sodium channel currents were measured using standard patch-clamp techniques (11). Cells were superfused with a 130 mM sodium external solution. The micropipettes were filled with an internal CsCl solution. The internal Cs⁺ blocked the endogenous K⁺ channels in the HEK-293-EBNA cells. Under these recording conditions, the inward sodium current was the only ionic current recorded.

Solutions. The solutions used in these experiments had the following composition (in mM): sodium external solution: 130 NaCl, 4 KCl, 1 CaCl₂, 5 MgCl₂, 5 HEPES, and 5 glucose (pH adjusted to 7.4 with NaOH); and Cs⁺ micropipette solution: 130 CsCl, 1 MgCl₂, 5 MgATP, and 10 HEPES (pH adjusted to 7.2 with CsOH). All experiments were performed at room temperature (20–22°C).

Recording techniques. Whole cell recordings were performed with an Axopatch-200A (Axon Instruments, Burlingame, CA) or EPC-10 (List Medical, Darmstadt, Germany) patch-clamp amplifier. Whole cell sodium channel currents were recorded with 0.5- to 1.5-M Ω microelectrodes coated with a hydrophobic elastomer (Sylgard 184) to their tips. Series resistance and capacity transient were compensated using standard techniques. At the beginning of each experiment, adequacy of voltage control was assessed as previously described (7). Whole cell currents were filtered at 10 kHz and digitized at 25–40 kHz. The holding potential was set at –100 mV.

The *G*-*V* relationship was determined by application of 20-ms pulses from a holding potential of –100 mV to test potentials of –80 to +40 mV. The amplitude of the test potential was incremented in 5-mV steps. Steady-state fast inactivation was determined using 500-ms conditioning pulses from –130 to –40 mV followed by 10-ms test pulses to –20 mV. The recovery from fast inactivation was determined using twin-pulse protocols (13). We also determined the rate of onset and recovery from intermediate inactivation using twin pulse protocols. From a holding potential of –100 mV, 0.5- to 5,000-ms conditioning pulses were applied to –20 mV. A 100-ms interval at –100 mV permitted recovery from fast inactivation. The sequence was completed with a 10-ms test pulse to –20 mV. To assess the kinetics of recovery from intermediate inactivation, a 2,000-ms conditioning pulse was applied from the holding potential to –20 mV. Test pulses were then applied at recovery intervals of 100–10,000 ms. We determined use-dependent reduction of the sodium current by the application of trains of sixty 50- and 100-ms pulses at interpulse intervals of 50, 100, 200, 300, 400, and 1,000 ms.

Data analysis. Whole cell sodium channel currents were analyzed with Clampfit 8.1 and custom software developed in our laboratory (7). Inactivation-voltage and *G*-*V* relationships were fit to a standard Boltzmann equation of the form: $h_{\infty, m_{\infty}} = 1 / \{1 \pm \exp[(V - V_{1/2})/k]\}$, where h_{∞} is the inactivation variable, m_{∞} is the activation variable, *V* is membrane potential, $V_{1/2}$ is the potential at which h_{∞} or $m_{\infty} = 0.5$, and *k* is the slope factor.

The development and recovery from inactivation were fit to a single exponential function: $I(t) = I_{\infty} [1 - \exp(-t/\tau)]$, where $I(t)$ is the current at time *t*, I_{∞} is the initial current or the steady-state current, and τ is the inactivation time constant.

Values are reported as means \pm SE, unless otherwise stated. Comparisons were made with unpaired or paired *t*-tests, as appropriate; $P < 0.05$ was considered significant.

Simulations. Computer simulations are useful to link experimentally observed channel dynamics to clinically observed phenomena such as changes in the electrocardiogram (ECG). Three separate, but related, simulation studies were performed using the experimental data for the WT, Δ K1479, and Δ K1500 mutations. All studies used the Dynamic Luo-Rudy (LRD) model to describe ion channel dynamics (26). The sodium current in the LRD model, however, was replaced by the empiric equations derived from experiments on WT, Δ K1479, and Δ K1500 sodium channels:

$$I_{Na} = \bar{G}_{Na} m^3 h [V_m - E_{Na}]$$

where V_m is membrane potential. The sodium reversal potential (E_{Na}) for all models was 71 mV, and the maximum sodium activation (\bar{G}_{Na}) was nominally set to 16 mS/cm². The dynamics of the *m* and *h* gates are described by differential equations:

$$dm/dt = (m - m_{\infty})/\tau_m \quad dh/dt = (h - h_{\infty})/\tau_h$$

where steady-state activation (m_{∞}) and inactivation (h_{∞}) are described by the standard Boltzmann distribution:

$$h_{\infty}, m_{\infty} = 1 / [1 \pm e^{(V_m - V_{1/2})/k}]$$

Table 1 shows the values used for $V_{1/2}$ and *k* in the simulations.

Activation time constants for WT and the mutant channels were fit to the same function:

$$\tau_m = \frac{0.0101}{\frac{0.0005(V_m + 77.0538)}{1 - e^{-0.1753(V_m + 77.0538)}} + 1.5043 \times 10^{-5} e^{-V_m/11.8696}}$$

The inactivation time constants are described in a piece-wise fashion to fit the experimental data as follows:

WT

if $V_m > -57.7$ mV

$$\tau_h = 3.1521 \times [1 + e^{-(V_m + 47.5939)/11.1719}]$$

else

$$\tau_h = \frac{1.2437}{0.0276e^{-(V_m + 86.4148)/10.9567} + 12.9885e^{0.0933V_m} + 11.3556e^{0.0933V_m}}$$

Δ K1479

if $V_m > -52.78$ mV

$$\tau_h = 2.7082 \times [1 + e^{-(V_m + 48.3208)/12.4224}]$$

else

$$\tau_h = \frac{1.7168}{0.0395e^{-(V_m + 80.68)/13.5522} + 8.6258e^{0.0782V_m} + 7.2339e^{0.0782V_m}}$$

Δ K1500

if $V_m > -25.5$ mV

$$\tau_h = 2.7402 \times [1 + e^{-(V_m + 74.3126)/4.7944}]$$

else

$$\tau_h = \frac{2.6987}{0.0536e^{-(V_m + 78.7396)/13.8114} + 0.8958e^{0.0235V_m} + 0.8954e^{0.0235V_m}}$$

Table 1. Steady-state activation and inactivation parameters used for simulation of sodium channel dynamics in wild-type, $\Delta K1479$, and $\Delta K1500$ mutants

	WT	$\Delta K1479$	$\Delta K1500$
<i>m</i>			
<i>k</i>	5.1	8.1	10.1
$V_{1/2}$	-36.8	-24.5	-21.4
<i>h</i>			
<i>k</i>	-5.6	-5.9	-6.3
$V_{1/2}$	-85	-79.4	-94

Units are mV. WT, wild type; *m*, activation parameter; *h*, inactivation parameter; *k*, slope factor; $V_{1/2}$, potential at which *m* or *h* is 0.5.

All simulations were performed using a semi-implicit Crank-Nicholson scheme with a $\Delta t = 0.01$ ms. The relationship between simulated and measured current is included in supplemental Fig. 1.

The first simulation was conducted to determine the impact of the mutations on the action potential of the various cell types that compose the human left ventricle. A uniform one-dimensional 2-cm cable ($\Delta x = 0.01$ cm) of uniformly coupled (1 mS/cm) cells was simulated to derive action potential characteristics. Cables were composed entirely of epicardial, M, or endocardial cells (26) with WT, $\Delta K1479$, or $\Delta K1500$ sodium channel dynamics. The nominal LRD model is for epicardial cells. The formulation for other cell types is created by changing the maximal conductance of I_{to} (\bar{G}_{to}) to 0.1 and 0 mS/cm for M and endocardial cells, respectively, and the maximal conductance of I_{ks} (\bar{G}_{ks}) to 0.2 mS/cm for both M and endocardial cells as previously described (8). Propagation was initiated by a 1-Hz suprathreshold current stimuli at one end of the cable (0 cm). Action potentials from the center of the cable (1 cm) at the 20th beat were recorded for analysis to minimize the stimulus artifact, boundary effects, and drift in ionic concentrations. Conduction velocities were computed from the difference in activation times (time of maximum upstroke velocity) at 0.5 and 1.5 cm along the cable.

The second simulation was conducted to determine the possible impact of the mutations on the ECG. Because simulation of a human heart and torso requires excessive computational expense, a pseudo-ECG (pECG) was simulated using a one-dimensional cable model of the human left ventricular wall. The pECG was derived from the volume conductor field generated by the action potentials propagating along the cable. The pECG was computed as the extracellular potential (ϕ) using the following relationship:

$$\phi = a^2/4\sigma_e \int (-\partial V_m/\partial x) \times [\nabla(1/r)]$$

$$r = [(x - x')^2 + (y - y')^2 + (z - z')^2]^{1/2}$$

where *a* is the radius of the cable, σ_e is the extracellular conductivity, *r* the distance from the recording point to the source element, and *x*, *y*, and *z* are the rectangular co-ordinate axes (8, 18). The action potential sources (V_m) were derived from a one-dimensional cable (1.65 cm) that was divided into epicardial (0–0.6 cm), M (0.6–1.05), and endocardial (1.05–1.65) regions. Propagation was initiated by a 1-Hz suprathreshold current stimuli at the endocardial end of the cable (1.65 cm). The pECG was computed as the extracellular potential 1 cm from the epicardial end of the cable (-1 cm) for the WT and $\Delta K1479$ and $\Delta K1500$ mutations with normal sodium channel excitability ($\bar{G}_{Na} = 16$ mS/cm²). In the clinic, the effect of a channel mutation on the ECG is often not immediately apparent but can be unmasked using a sodium channel blocker. The effect of low excitability on the pECG was simulated by decreasing \bar{G}_{Na} to 8 mS/cm² in the WT, $\Delta K1479$, and $\Delta K1500$ cables.

The third stimulation study aimed to determine the effects of shifts in the steady-state conductance and inactivation curves on conduction velocity. We performed these simulations since some mutations affect clinically observable phenomena (e.g., morphology of the ECG,

conduction velocities) by shifting the steady-state conductance and inactivation curves in either the depolarizing or hyperpolarizing direction. A 2-cm uniform cable made of WT epicardial cells (similar to study one) was used with the same stimulation protocol. The conduction velocity was computed in cables as $V_{1/2m}$ was varied between -10 and -60 mV and as $V_{1/2h}$ was varied between -30 and -140 mV. The WT activation and inactivation time constants were held constant.

RESULTS

Sodium channel mutations that produce the Brugada syndrome reduce the sodium current as a result of decreased expression of functional channels or changes in channel kinetics. Both the WT and the K1479 deletion ($\Delta K1479$) mutant channels expressed robust current in HEK-293-EBNA. Mean peak current density was 404 ± 87 pA/pF ($n = 11$) in the WT and 318 ± 44 pA/pF ($n = 10$) in the $\Delta K1479$ mutant. We compared the steady-state fast inactivation and activation of the two channel types. Summary data are presented in Fig. 1, *A* and *B*. The steady-state inactivation curve was shifted in a depolarizing direction compared with the WT channel; $V_{1/2h}$ for the WT was -85 ± 1.1 mV ($n = 11$) and for the $\Delta K1479$ was -79.4 ± 1.2 mV ($n = 10$, $P = 0.002$). This 5.6-mV depolarizing shift will increase the availability of the sodium channel at the normal resting potential of approximately -90 mV. The slope factor was unchanged; k_h for the WT was -5.6 ± 0.2 mV and for $\Delta K1479$ was -5.9 ± 0.3 mV ($P = 0.24$). The *G-V* relationship was also shifted in a depolarizing direction; $V_{1/2m}$ for the WT was -36.8 ± 0.8 mV and $V_{1/2m}$ for the $\Delta K1479$ mutant was -24.5 ± 1.3 mV ($P = 0.001$). This positive shift of the *G-V* relationship will delay the onset of channel activation. In the representative current recordings illustrated in Fig. 1, *C* and *D*, the current activated at -40 mV is 33% of that activated at -20 mV for the WT channel. In the case of the $\Delta K1479$ channel only, 15% of current is activated at -40 mV. The slope factor was increased; k_m for WT was 5.1 ± 0.3 mV and for $\Delta K1479$ 8.1 ± 0.2 mV ($P = 0.001$). The slope factor is the number of millivolts required for an *e*-fold increase in activation. Therefore, the increased slope factor indicates reduced voltage dependence of activation. Marked, although similar increases in both the rate of onset (β_h) and recovery (α_h) from inactivation may exert substantial influence on conduction, they produced little change in steady-state inactivation [$h_\infty = 1/(1 + \beta/\alpha)$]. At most potentials, the processes of development and recovery from inactivation are occurring simultaneously (both α_h and β_h have finite values). At potentials positive to threshold, the net kinetic change is the development of inactivation ($\beta_h \gg \alpha_h$). At most subthreshold potentials, recovery from inactivation predominates ($\alpha_h > \beta_h$). We compared the inactivation of the current at potentials positive to the activation threshold and determined the rates of recovery at subthreshold potentials using a two-pulse protocol (13). The relaxation of the current was well fit by single exponentials. Representative currents for the WT and $\Delta K1479$ channels are shown in Fig. 2, *A* and *B*. At potentials close to threshold, relaxation of the WT current was faster. However, at potentials positive to -20 mV, the rates of current relaxation were similar (Fig. 2*C*). At most potentials, the $\Delta K1479$ channels recovered from closed-state inactivation faster than the WT channels (Fig. 2*D*). These detailed kinetic changes in fast inactivation do not translate into a reduction of channels available for activation during the action potential.

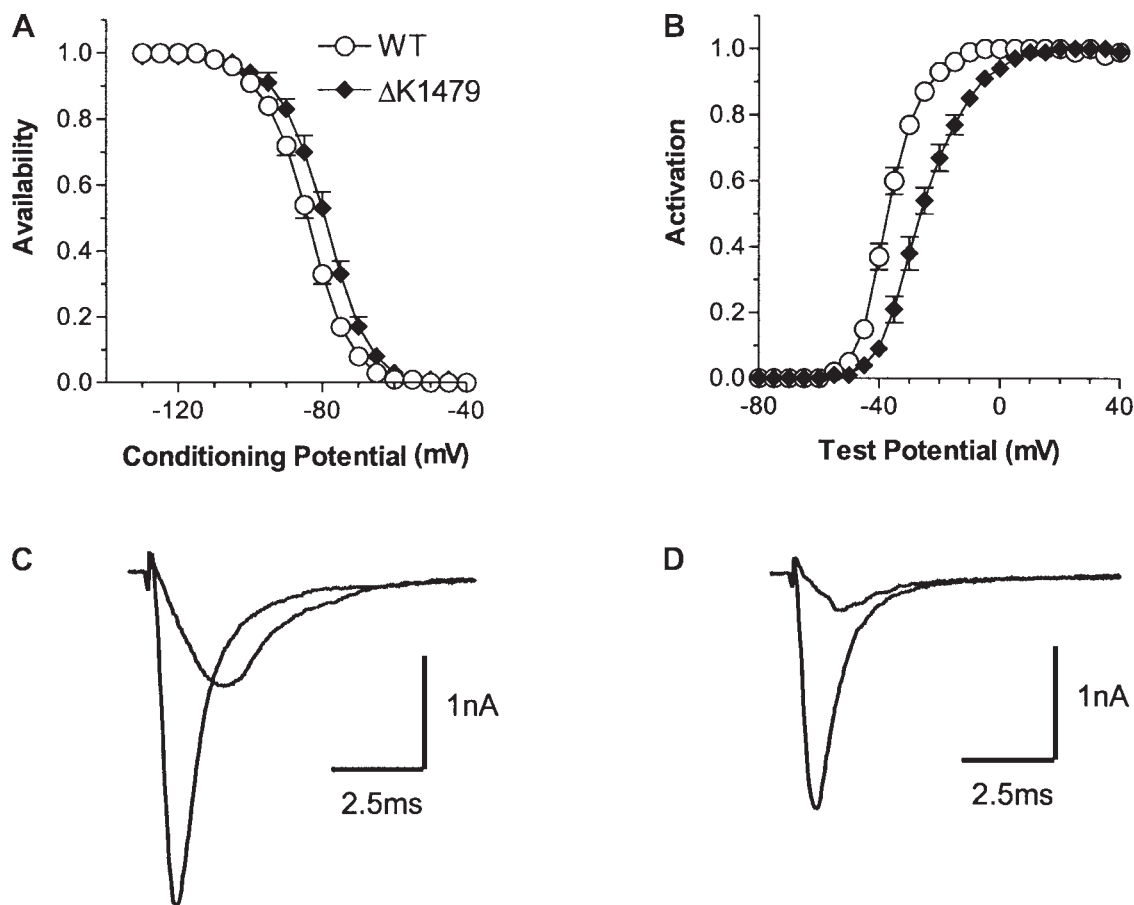


Fig. 1. Comparison of the steady-state fast inactivation, activation, and kinetics of the sodium current in cells expressing the wild-type (WT) and Δ K1479 mutant channels. *A*: summary data of channel availability as a function of membrane potential. Potential of half-inactivation ($V_{1/2h}$) was -85 ± 1.1 and -79.4 ± 1.2 mV for the WT and Δ K1479 channels, respectively; the slope factor was -5.6 ± 0.2 and -5.9 ± 0.3 mV. *B*: channel activation plotted as a function of test potential. Potential of half-activation ($V_{1/2m}$) was -36.8 ± 0.8 and -24.5 ± 1.3 mV for the WT and Δ K1479 channels, respectively. *C* and *D*: WT (*C*) and Δ K1479 (*D*) membrane currents in response to voltage steps to -40 and -20 mV from a holding potential of -100 mV.

The steady-state relationships (G - V , h_{∞} - V) are customarily determined at slow (unphysiological) stimulus frequencies to assure complete recovery between voltage-clamp runs. Certain Brugada syndrome-associated mutations have their major influence on slower (intermediate) components of sodium channel inactivation. The intermediate and slow components of inactivation have distinctly different molecular bases from fast inactivation. Therefore, we describe the development and recovery from intermediate inactivation separately from the kinetics of fast inactivation. We determined the rate of onset and of recovery from intermediate inactivation using a twin pulse protocol. Summary data are presented in Fig. 3. Intermediate inactivation developed with a time constant of $1,590 \pm 207$ ms ($n = 5$) in the WT channel and $3,633 \pm 316$ ms ($n = 5$, $P = 0.001$) in the Δ K1479 mutant channel. Recovery from inactivation was faster in the WT channel, $\tau_{WT} = 298 \pm 38$ ms and $\tau_{\Delta K1479} = 527 \pm 75$ ms ($P = 0.01$). To determine the impact these changes in intermediate inactivation would have on the sodium current during a series of consecutive action potentials, we used trains of 100-ms pulses at interpulse intervals of 50, 100, 200, 300, 400, and 1,000 ms. For clarity, we present the results at interpulse intervals of 50, 100, and 1,000 ms only in Fig. 4, *A* and *B*. At the shortest interpulse interval of 50 ms, the current during the last pulse of the train was 0.83 ± 0.4 ($n = 4$) that of the first pulse of the train for the WT channel;

for the Δ K1479 mutant channel the fractional current was 0.89 ± 0.3 ($n = 5$).

We simulated the effects of the WT, Δ K1479, and Δ K1500 mutation on the action potential and pECG. We included Δ K1500 mutant channel in the simulations since our prior studies of this mutant showed gating effects that contrast with those of the Δ K1479 mutant channel. Like the Δ K1479 mutant, $V_{1/2m}$ was also shifted in a depolarizing direction, but $V_{1/2h}$ was shifted in a hyperpolarizing direction by 13.4 mV with the Δ K1500 mutant. The combined effects of these shifts are predicted to produce even greater conduction slowing than the Δ K1479 mutation. Figure 5 shows simulated action potentials and pECGs of epicardial, M, and endocardial regions of WT, Δ K1479, and Δ K1500 cells under conditions of normal and reduced excitability. Action potential durations (APDs) were 208, 225, and 230 ms in the epicardial, M, and endocardial regions of WT cells, respectively. There is an epicardial-to-endocardial gradient, and a slightly positive T wave in the pECG (Fig. 5*C*). For the low excitability case, the conduction velocity is slowed enough that repolarization takes place in roughly the same order as depolarization (endocardial, M, and epicardial region), resulting in a slightly negative T wave. Under conditions of normal excitability, the APDs for the Δ K1479 mutant are similar to WT. However, under con-

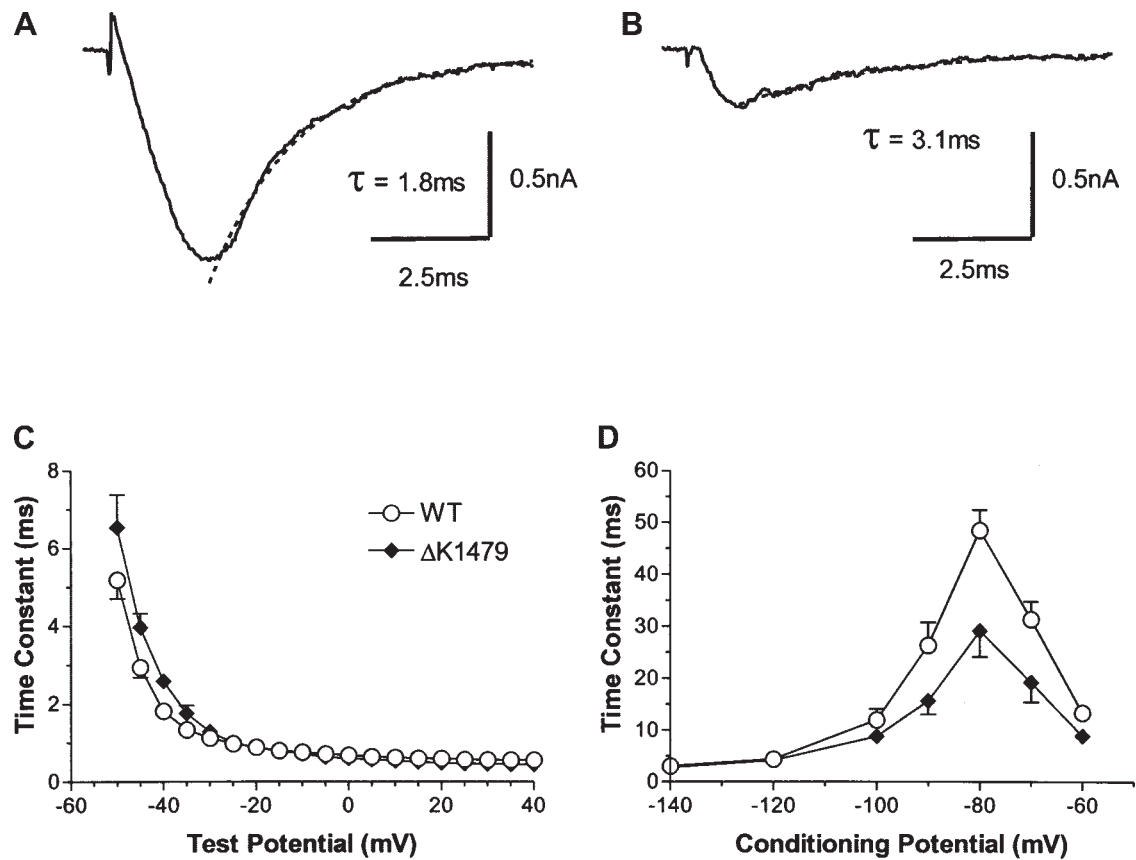


Fig. 2. Inactivation kinetics of WT and Δ K1479 mutant channels. *A* and *B*: membrane current in response to depolarization to -40 mV in the WT (*A*) and Δ K1479 mutant (*B*) channels. For both channel types, current relaxation was well fit by a single exponential. *C*: summary data over a wide range of potential. The time constant of relaxation of the Δ K1479 mutant channel current is significantly larger than the WT at test potentials of -45 , -40 , and -35 mV. *D*: time constants for the recovery or development of inactivation using a two-pulse protocol. Time constants for the Δ K1479 mutant are smaller than those of the WT channel at potentials of -80 , -70 , and -60 mV.

ditions of reduced excitability, a significant APD gradient is unmasked as a result of conduction slowing. Repolarization occurs earliest in the endocardium, the T wave in pECG is inverted and the QT interval prolonged. Even in the baseline state, the Δ K1500 mutant shows significant APD gradients that are in fact reversed: 330, 277, and 251 for the epicardial, M, and endocardial cells. The T wave is inverted and the QT interval prolonged in the baseline state. The overall prolongation of the APD is consistent with the clinical occurrence of LQTS in patients with the Δ K1500 mutation and a threefold increase in the late component during heterologous expression (9). The epicardial cell was most susceptible to prolongation of the APD with an increase in the late component of the sodium current. The reverse APD gradient accounts for the deep inversion of the T wave and may also account for the T wave changes observed in the proband with the Δ K1500 mutation (9). Repolarization of the M and endocardial cell is further delayed ~ 100 ms under conditions of reduced excitability, and the T wave inversion and QT interval prolongation persist. Although not widely reported, QTc prolongation during provocative testing with sodium channel blockers appears to be an “electrocardiographic hallmark” of the syndrome (17).

Figure 6, *A* and *B*, shows activation times and the APD at the indicated positions along the cable. At each point, the activation time is the time of occurrence of dV/dt_{max} . Zero centimeters corresponds to the endocardium (the stimulation site) and 1.65 cm

the recording site. Under conditions of normal excitability, activation times are delayed uniformly along the cable and is latest for Δ K1500 mutant. Under conditions of reduced excitability, activation times are markedly delayed in the Δ K1479 and Δ K1500 mutants and are nonuniform with the Δ K1479 and Δ K1500 mutants. The spatial distribution of the APD is significantly exaggerated in Δ K1479 and Δ K1500 (Fig. 6*B*).

Figure 7 shows simulations of the relationship between conduction velocity, θ , and the potentials of half-activation and inactivation ($V_{1/2m}$ and $V_{1/2h}$, respectively). Action potentials were initiated at approximately the same potential (-88 mV). As $V_{1/2m}$ is made more positive and/or $V_{1/2h}$ is made more negative, θ declines. The decline in θ is most dramatic when depolarizing shifts in $V_{1/2m}$ and hyperpolarizing shifts in $V_{1/2h}$ are present. The mutation Δ K1500 has this combination of parameters. On the other hand, the depolarizing shift of $V_{1/2h}$ of the Δ K1479 mutant moves the conduction velocity to a less steep segment of the θ - $V_{1/2h}$ relationship. The simulations also show a surprising result: conduction is maintained at very negative values of $V_{1/2h}$ provided that $V_{1/2m}$ is also very negative, e.g., -60 mV.

DISCUSSION

We have analyzed the functional effects of the Δ K1479 mutation using whole cell recordings and computer simulations

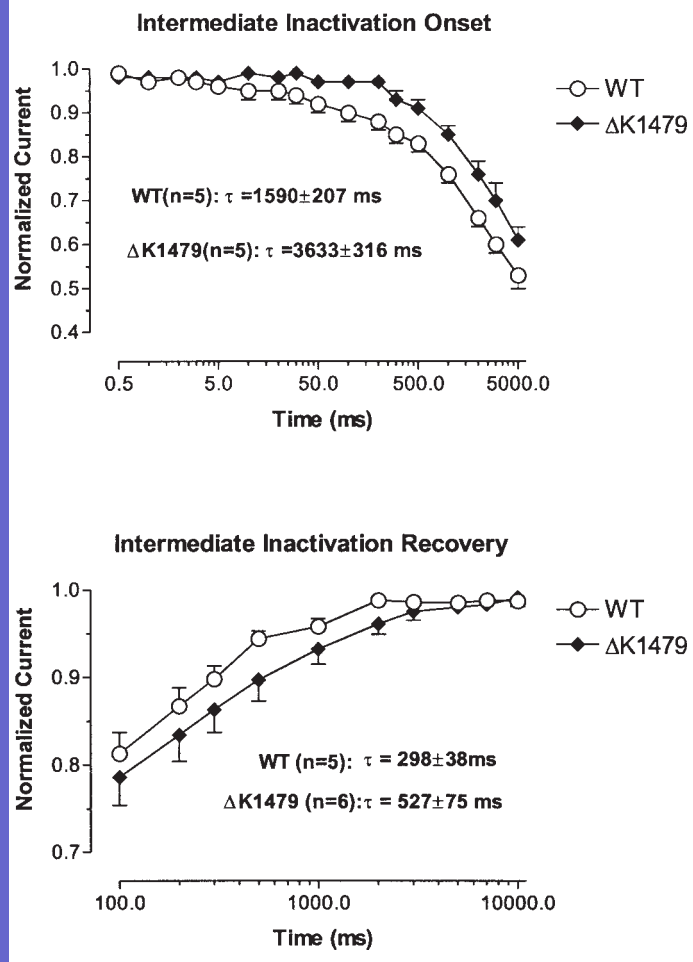


Fig. 3. Onset and recovery from intermediate inactivation in WT and Δ K1479 mutant channels. *Top*: normalized test-pulse currents plotted against conditioning pulse duration on a log scale. In the individual experiments, onset of intermediate inactivation was fit by a single exponential function. *Bottom*: normalized test pulse current as a function of diastolic interval plotted on a log scale. The holding potential was -100 mV.

of the action potential and conduction in a one-dimensional cable. The results obtained were related to the clinical phenotype of Brugada syndrome and conduction disease. These studies are of potential interest for the following two reasons: the insight that they may provide on the role of the charged residues in the III/IV interdomain linker and the relationship between changes in channel gating and the simultaneous occurrence of Brugada syndrome and PCCD.

The III/IV interdomain linker is highly conserved and contains 15 charged residues grouped in two α -helical clusters in a hairpin motif (6). K1479 is located in the first cluster (which comprises residues 1473–1479), whereas K1500 is located in the second and longer cluster. The deletion of K1479 shifts the potential of half-activation $+12$ mV. This effect on activation is similar to that of the deletion of K1500. However, in contrast to the deletion of K1500, the deletion of K1479 produces a depolarizing shift in channel inactivation, suggesting that the roles of two clusters on channel inactivation are not equivalent. In general, the central role of the III/IV interdomain linker in inactivation is well recognized. In particular, the α -helical clusters are believed to form a rigid scaffold to present the hydrophobic inactivation amino acid triplet IFM to its receptor

site. In this process, inactivation is coupled to activation, probably through interaction with the charged residues in the S₄ transmembrane segment (16). The difference in length of the α -helical clusters may signify differing roles in gating coupling. K1479 is a charged residue of a triplet KKK. The effect of Δ K1479 on activation is consistent with the mutation analysis of this triplet in rat (r)Nav 1.2, which exhibited the most dramatic effects on activation gating (a $+12$ -mV shift in the potential of half-activation) when the charges were reversed . . . KKK/EEE (16).

The simultaneous occurrence of Brugada syndrome and conduction system disease can both be explained by conduction slowing. Our simulations for Δ K1479 channels (Fig. 5) capture the occurrence of a slight transmural voltage gradient only during late *phase 0* and *phase 1* of the simulated action potentials. We were struck by the lack of large APD (*phase 3*) gradients predicted in other simulations, e.g., Dumaine et al. (5). A careful review of those results shows that the magnitude of the transient outward current is increased severalfold or the inactivation kinetics of sodium current is markedly accelerated above that observed experimentally (8). As illustrated in Fig. 5, the kinetic changes that we observed with the Δ K1479 are sufficient to produce J point elevation. The more dramatic ECG effect of “apparent right bundle branch” may truly be a reflec-

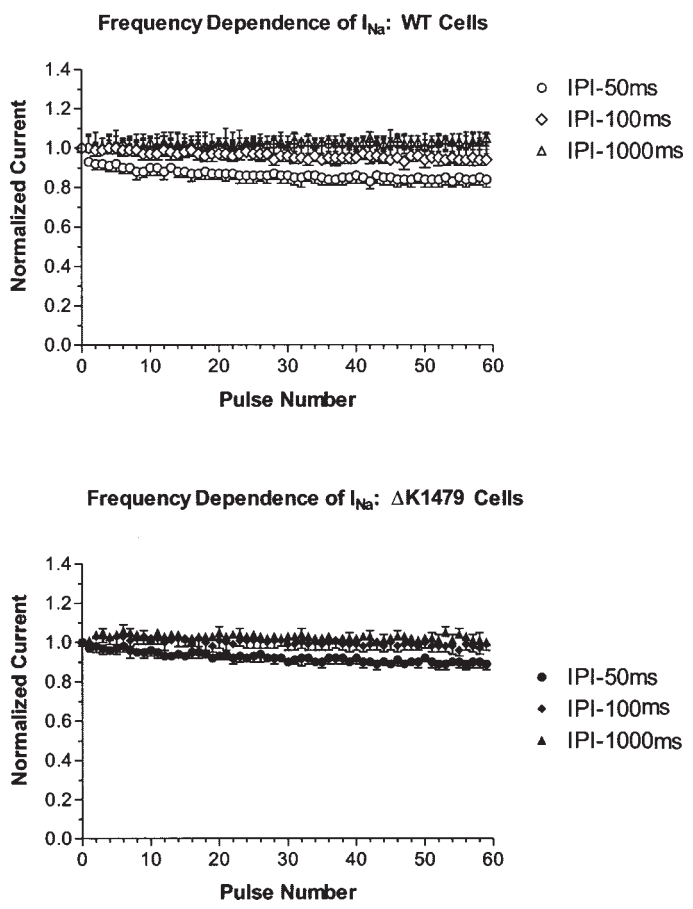


Fig. 4. Membrane current in response to pulse-train stimulation in WT and Δ K1479 channels. Trains of 100-ms pulses were applied at interpulse intervals (IPI) of 50, 100, and 1,000 ms. Normalized currents are plotted against the pulse number. The error bars were about the same size as the symbols for each pulse sequence. I_{Na} , sodium current.

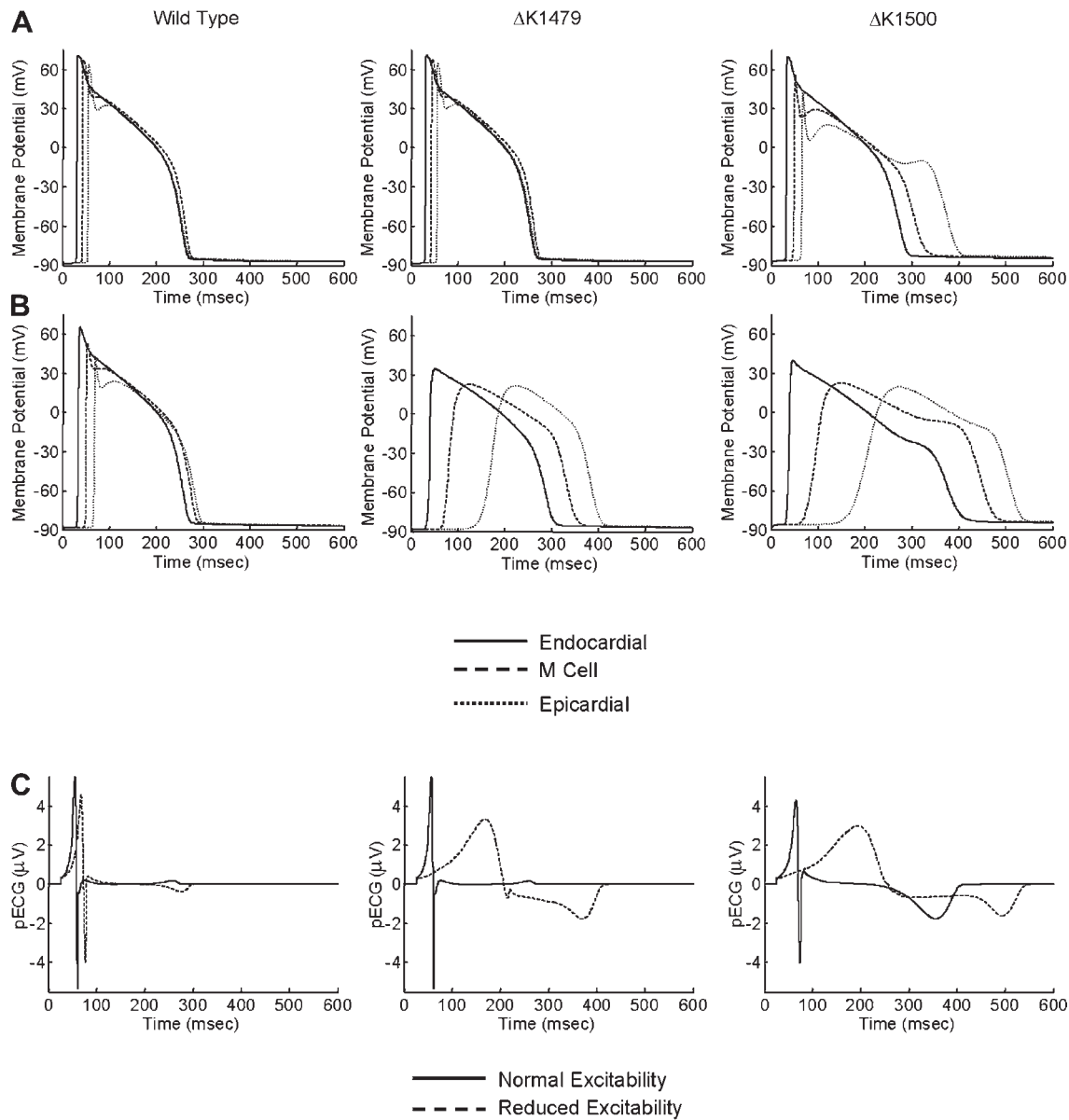


Fig. 5. Simulations of the action potentials in the epicardial, M, and endocardial regions of the ventricular wall for the WT, $\Delta K1479$, and $\Delta K1500$ channels. *A*: action potential simulations under normal conditions for the endocardial, M, and epicardial regions. *B*: action potentials under conditions of reduced excitability. Maximum sodium activation was reduced from 16 to 8 mS/cm² for reduced excitability case. *C*: pseudo-electrocardiograms (pECGs).

tion of right-sided conduction delay rather than significant APD gradients. A recently published study by Coronel et al. (4) supports this conclusion. They performed a detailed in vitro study of the heart removed from a patient with Brugada syndrome and intractable ventricular tachycardia/fibrillation. Direct mapping documented marked conduction delay in the right ventricular outflow tract. Marked heterogeneities in repolarization consistent with loss of the action potential dome in the epicardium were not observed. The occurrence of intraventricular conduction delay, e.g., prolongation of the HV interval, is a mark of an underlying sodium channel mutation in Brugada syndrome (24).

We now briefly discuss the relationship between our findings and those studies that examine the occurrence of Brugada syndrome and PCCD. Mutations in the cardiac sodium channel gene may cause LQTS, Brugada syndrome, PCCD, or a com-

bination of these syndromes (15). Increased reversibility of fast inactivation with enhancement of the late component of sodium current is almost uniformly the cause of LQTS. On the other hand, conduction slowing as a result of expression of nonfunctional channels, or channels with altered gating, is a common basis for sodium channel-associated Brugada syndrome and PCCD. Which of these two disease phenotypes will be present is not clear and may vary in different individuals having the same sodium channel mutation. Tan et al. (25) described a kindred with conduction system disease associated with a glycine-to-cysteine mutation in the I/II interdomain linker of the cardiac sodium channel gene G514C. Biophysical analysis of the heterologously expressed mutant channel showed a +10-mV shift of the potential of half-activation and a +7-mV shift in the potential of half-inactivation. They presented simulations that suggest that the counterbalancing

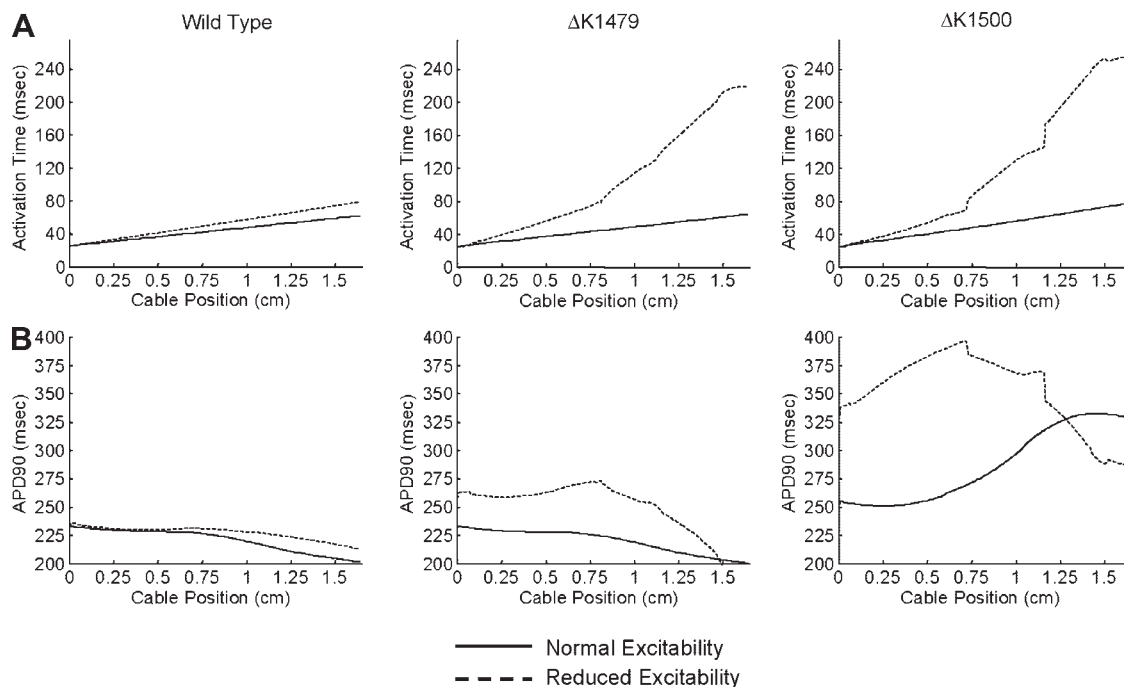


Fig. 6. *A* and *B*: activation times (*A*) and action potential duration (APD; *B*) along the cable for WT, $\Delta K1479$, and $\Delta K1500$ mutant channels. Stimulation was initiated at the endocardium. The activation time is the time of occurrence of dV/dt_{max} at each point along the cable. The APD plot is the functional APD, i.e., with all cells coupled.

effects of the activation and inactivation voltage shifts would produce PCCD only. The findings reported in our study show that very similar shifts in the voltage dependence of activation and inactivation can produce Brugada syndrome. The simulation showed that the qualitative changes in action potential and pECG can also be observed with the positive shift in both parameters.

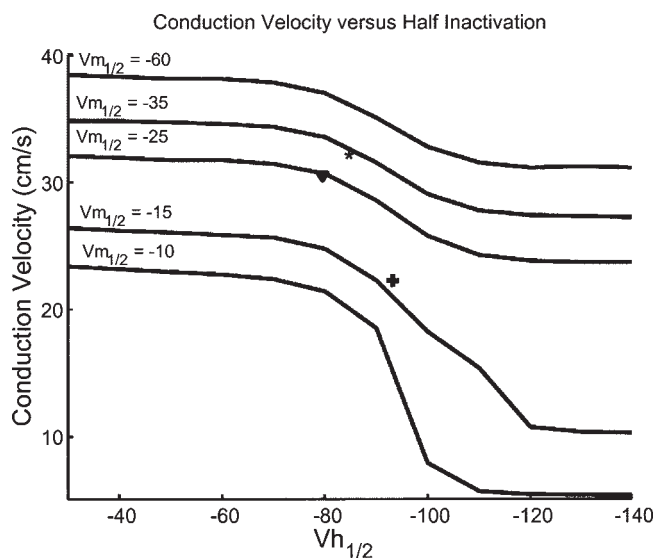


Fig. 7. Simulations of the relationship between conduction velocity and $V_{1/2h}$. Contours for values of $V_{1/2m}$ from -60 to -10 mV are also shown. The simulations started from the rest potential, which was approximately -88 mV for all values of $V_{1/2h}$. The conduction velocity declines as $V_{1/2h}$ is made more negative, and the rate of the decline is accentuated at depolarized values of $V_{1/2m}$, e.g., -15 and -10 mV.

The most severe sodium channel defect is haploinsufficiency. Both PCCD and Brugada syndrome are observed with mutations that produce haploinsufficiency (3, 21). We conclude that other factors determine the phenotype in a kindred. The proband of the kindred and the other affected individual presented by Tan et al. (25) were 3 and 6 yr old when they presented with PCCD (25). Brugada syndrome usually presents in the fourth decade of life. Although the disorder is inherited as an autosomal dominant, $\sim 80\%$ of the affected individuals are males (2). The affected individuals described by Tan et al. were both females. Kyndt et al. (14) described a 45-member family with Brugada syndrome, PCCD, and the mutation G1406R in $Na_{V1.5}$. All four family members with Brugada syndrome were males, and six of seven members with PCCD were females.

For sodium channel mutations that do produce functional channels, the most severe defect combines a positive shift in the potential of half-activation and a negative shift in the potential of half-inactivation. This combination of gating defects may produce Brugada syndrome and conduction defects at several levels, including the sinoatrial and atrioventricular nodes and the His-Purkinje system (9). On the other hand, Akai et al. (1) described a family with ventricular fibrillation and a mutation S1710L in $Na_{V1.5}$. The 39-yr-old proband did not have S-T segment elevation in V_{1-3} at rest or after disopyramide administration. Right Bundle Branch Block developed during an increase in heart rate. The S1710L mutation produced a $+18.7$ -mV shift in $V_{1/2m}$ and a -21.7 -mV shift in $V_{1/2h}$. These changes would be predicted to produce Brugada syndrome. Phenotype-genotype correlations are best refined by inclusion of both genders, individuals of a range of ages or observations over time. This is borne out by a recent study by

Probst et al. (19). From a cohort of 40 probands with Brugada syndrome and sodium channel mutations, they identified 78 mutation carriers. Conduction disturbances were identified in 76% of males and 75% of female gene carriers. The conduction disturbance progressed with aging, and five gene carriers required pacemaker implantation.

GRANTS

This work was supported by National Heart, Lung, and Blood Institute Grant 2 RO1HL-067145-04.

REFERENCES

1. Akai J, Makita N, Sakurada H, Shirai N, Ueda K, Kitabatake A, Nakazawa K, Kimura A, and Hiraoka M. A novel *SCN5A* mutation associated with idiopathic ventricular fibrillation without typical ECG findings of Brugada syndrome. *FEBS Lett* 479: 29–34, 2000.
2. Antzelevitch C, Brugada P, Brugada J, Brugada R, Towbin JA, and Nademancee K. Brugada syndrome: 1992–2002. *J Am Coll Cardiol* 41: 1665–1671, 2003.
3. Chen Q, Kirsch GE, Zhang D, Brugada R, Brugada J, Brugada P, Potenza D, Moya A, Borggrefe M, Breithardt G, Prtoz-Lopez R, Wang Z, Antzelevitch C, Brien REO, Schulze-Bahr E, Keating MT, Towbin JA, and Wang Q. Genetic basis and molecular mechanism for idiopathic ventricular fibrillation. *Nature* 392: 293–296, 1998.
4. Coronel R, Casini S, Koopmann TT, Wilms-Schopman FJG, Verkerk AO, de Groot JR, Bhuiyan Z, Bezzina CR, Veldkamp MW, Linnenbank AC, van der Wal AC, Tan HL, Brugada P, Wilde AAM, and de Bakker JMT. Right ventricular fibrosis and conduction delay in a patient with clinical signs of Brugada syndrome: a combined electrophysiological, genetic, histopathologic, and computational study. *Circulation* 112: 2769–2777, 2005.
5. Dumaine R, Towbin JA, Brugada P, Vatta M, Nesterenko DV, Nesterenko VV, Brugada J, Brugada R, and Antzelevitch C. Ionic mechanisms responsible for the electrocardiographic phenotype of the Brugada syndrome are temperature dependent. *Circ Res* 85: 803–809, 1999.
6. Fozzard H and Hanck DA. Structure and function of voltage-dependent sodium channels: Comparison of brain II and cardiac isoforms. *Physiol Rev* 76: 887–926, 1996.
7. Gilliam FRI, Starmer CF, and Grant AO. Blockade of rabbit atrial sodium channels by lidocaine: Characterization of continuous and frequency-dependent blocking. *Circ Res* 65: 723–739, 1989.
8. Gima K and Rudy Y. Ionic current basis of electrocardiographic waveforms. *Circ Res* 90: 889–896, 2002.
9. Grant AO, Carboni MP, Neplioueva V, Starmer CF, Memmi M, Napolitano C, and Priori S. Long QT syndrome, Brugada syndrome, and conduction system disease are linked to a single sodium channel mutation. *J Clin Invest* 110: 1201–1209, 2002.
10. Gussak I, Antzelevitch C, Bjerregaard P, Towbin JA, and Chaitman BR. The Brugada syndrome: clinical, electrophysiologic and genetic aspects. *J Am Coll Cardiol* 33: 5–15, 1999.
11. Hamill OP, Marty A, Neher E, Sakmann B, and Sigworth F. Improved patch-clamp techniques for high-resolution current recording from cell and cell-free membrane patches. *Pflugers Arch* 391: 85–100, 1981.
12. Higuchi R. Recombinant PCR. In: *PCR Protocols: A Guide to Methods and Applications*, edited by Innis MA. San Diego, CA: Academic, 1990, p. 177–183.
13. Hodgkin AL and Huxley AF. The dual effect of membrane potential on sodium conductance in the giant axon of loligo. *J Physiol* 116: 497–506, 1952.
14. Kyndt F, Probst V, Potet F, Demolombe S, Chevallier JC, Baro I, Moisan JP, Boisseau P, Schott JJ, Escande D, and Marec HL. Novel *SCN5A* mutation leading either to isolated cardiac conduction defect or Brugada syndrome in a large French family. *Circulation* 104: 3081–3086, 2001.
15. Moric E, Herbert E, Trusz-Gluzza M, Filipceki A, Mazurek U, and Wilczok T. The implications of genetic mutations in the sodium channel gene (*SCN5A*). *Europace* 5: 325–334, 2003.
16. Patton DE, West JW, Catterall WA, and Goldin AL. Amino acid residues required for fast Na^+ -channel inactivation: Charge neutralizations and deletions in the III-IV linker. *Proc Natl Acad Sci USA* 89: 10905–10909, 1992.
17. Pitzalis MV, Anacleiro M, Mastropasqua F, Sorrentino S, Manghisi A, and Rizzon P. QT-interval prolongation in right precordial leads: an additional electrocardiographic hallmark of Brugada syndrome. *J Am Coll Cardiol* 42: 1632–1637, 2003.
18. Plonsey R and Barr RC. Extracellular fields. In: *Bioelectricity: A Quantitative Approach*. New York: Plenum, 2000, p. 217–243.
19. Probst V, Allouis M, Sacher F, Pattier S, Babuty D, Mabo P, Mansourati J, Victor J, Nguyen JM, Schott JJ, Boisseau P, Escande D, and Le Marec H. Progressive cardiac conduction defect is the prevailing phenotype in carriers of a Brugada syndrome *SCN5A* mutation. *J Cardiovasc Electrophysiol* 17: 270–275, 2006.
20. Rohl CA, Boeckman FA, Baker C, Scheuer T, Catterall WA, and Klevit RE. Solution structure of the sodium channel inactivation gate. *Biochemistry* 38: 855–861, 1999.
21. Schott JJ, Alshinawi C, and Kyndt F. Cardiac conduction defects associate with mutations in *SCN5A*. *Nature Genet* 23: 20–21, 1999.
22. Schulze-Bahr E, Eckardt L, Breithardt G, Seidl K, Wichter T, Wolpert C, Borggrefe M, and Haverkamp W. Sodium channel gene (*SCN5A*) mutations in 44 index patients with Brugada syndrome: different incidences in familial and sporadic disease. *Human Mutation* 21: 651–652, 2003.
23. Sirota FL, Pascutti PG, and Anteneoda C. Molecular modeling and dynamics of the sodium channel inactivation gate. *Biophys J* 82: 1207–1215, 2002.
24. Smits JP, Eckardt L, Probst V, Bezzina CR, Schott JJ, Remme CA, Haverkamp W, Breithardt G, Escande D, Schulze-Bahr E, LeMarec H, and Wilde AA. Genotype-phenotype relationship in Brugada syndrome: electrocardiographic features differentiate *SCN5A*-related patients from non-*SCN5A*-related patients. *J Am Coll Cardiol* 40: 350–356, 2002.
25. Tan H, Bink-Boelkens M, Bezzina C, Viswanathan P, Beaufort-Krol G, van Tinteien P, van den Berg M, Wilde A, and Balsler J. A sodium-channel mutation causes isolated cardiac conduction disease. *Nature* 409: 1043–1047, 2001.
26. Viswanathan PC, Shaw RM, and Rudy Y. Effects of I_{Kr} and I_{Ks} heterogeneity on action potential duration and its rate dependence. *Circulation* 99: 2466–2474, 1999.
27. Wan X, Chen S, Sadeghpour A, Wang Q, and Kirsch G. Accelerated inactivation in a mutant Na^+ channel associated with idiopathic ventricular fibrillation. *Am J Physiol Heart Circ Physiol* 280: H354–H360, 2001.